Widespread air pollutants of the North China Plain during the Asian summer monsoon season: A case study

Jiarui Wu[1,3], Naifang Bei[2], Xia Li[1,3], Junji Cao[1*], Tian Feng[1], Yichen Wang[1], Xuexi Tie[1], and Guohui Li[1*]

[1]Key Lab of Aerosol Chemistry and Physics, SKLLQG, Institute of Earth Environment, Chinese Academy of Sciences, Xi'an, China
[2]School of Human Settlements and Civil Engineering, Xi'an Jiaotong University, Xi'an, Shaanxi, China
[3]University of Chinese Academy of Science, Beijing, China

[*]Correspondence to: Guohui Li (ligh@ieecas.cn) and Junji Cao (jjcao@ieecas.cn)

Supporting Information Section

The supporting information (SI) provides description about the WRF-CHEM model configuration, methodology, synoptic conditions, and model evaluations during the study episode.

Section SI-1 WRF-CHEM Model and Configuration

SI-1.1 WRF-CHEM Model

The WRF-CHEM used in this study includes a new flexible gas phase chemical module and the CMAQ aerosol module developed by US EPA (Li et al., 2010; Binkowski and Roselle, 2003). The wet deposition employs the method used in the CMAQ and the surface deposition of chemical species is parameterized following Wesely (1989). The photolysis rates are calculated using the FTUV (Li et al., 2005, 2011a), considering the effects of aerosols and clouds on photolysis.

The simulation of inorganic aerosols in the WRF-CHEM model adopts the ISORROPIA Version 1.7 (Nenes et al., 1998). The secondary organic aerosol (SOA) formation is calculated using a non-traditional SOA module. The volatility basis-set (VBS) modeling method applied in the module assumes that primary organic components are semi-volatile and photochemically reactive and are distributed in logarithmically spaced volatility bins. Detailed information about the volatility basis-set approach can be found in Li et al (2011b). The SOA formation from glyoxal and methylglyoxal is also parameterized as a first-order irreversible uptake by aerosol particles and cloud droplets.

SI-1.2 Model Configuration

The physical parameterizations include the microphysics scheme of Hong et al (Hong and Lim, 2006), the Mellor, Yamada, and Janjic (MYJ) turbulent kinetic energy (TKE) planetary boundary layer scheme (Janjić, 2002), the Unified Noah land-surface model (Chen and Dudhia, 2001), the Goddard longwave radiation scheme (Chou and Suarez, 2001) and the Goddard shortwave parameterization (Chou and Suarez, 1999). The NCEP 1° × 1° reanalysis data are used to obtain the meteorological initial and boundary conditions, and the meteorology has been nudged in the model simulation. The chemical initial and boundary conditions are interpolated from the 6h output of MOZART (Horowitz et al., 2003). The spin-up time of the WRF-CHEM model is 28 hours. The SAPRC-99 (Statewide Air Pollution Research Center, version 1999) chemical mechanism is used in the present study. The anthropogenic emissions are developed by Zhang et al. (2009), including contributions from agriculture, industry, power generation, residential, and transportation sources. The biogenic emissions are calculated online using the MEGAN (Model of Emissions of Gases and Aerosol from Nature) model developed by Guenther et al (2006).

Section SI-2 Methodology

SI-2.1 Factor Separation Approach

The formation of the secondary atmospheric pollutant, such as O_3, secondary organic aerosol, and nitrate, is a complicated nonlinear process in which its precursors from various emission sources and transport react chemically or reach equilibrium thermodynamically. Nevertheless, it is not straightforward to evaluate the contributions from different factors in a nonlinear process. The factor separation approach (FSA) proposed by Stein and Alpert (1993) can be used to isolate the effect of one single factor from a nonlinear process and has been widely used to evaluate source effects (Gabusi et al., 2008; Weinroth et al., 2008; Carnevale et al., 2010; Li et al., 2014a). The total effect of one factor in the presence of others can be decomposed into contributions from the factor and that from the interactions of all those factors.

Suppose that field $\boldsymbol{f}$ depends on a factor $\boldsymbol{\varphi}$:

$$\boldsymbol{f} = \boldsymbol{f}(\boldsymbol{\varphi})$$

The FSA decomposes function $\boldsymbol{f}(\boldsymbol{\varphi})$ into a constant part that does not depend on $\boldsymbol{\varphi}$ ($\boldsymbol{f}(\mathbf{0})$) and a $\boldsymbol{\varphi}$-depending component ($\boldsymbol{f}'(\boldsymbol{\varphi})$), as follows:

$$\boldsymbol{f}'(\mathbf{0}) = \boldsymbol{f}(\mathbf{0})$$

$$\boldsymbol{f}'(\boldsymbol{\varphi}) = \boldsymbol{f}(\boldsymbol{\varphi}) - \boldsymbol{f}(\mathbf{0})$$

Considering that there are two factors *X* and *Y* that influence the formation of secondary pollutants in the atmosphere and also interact with each other. Denoting $\boldsymbol{f}_{\boldsymbol{XY}}$, $\boldsymbol{f}_{\boldsymbol{X}}$, $\boldsymbol{f}_{\boldsymbol{Y}}$, and $\boldsymbol{f}_{\mathbf{0}}$ as the simulations including both of two factors, factor *X* only, factor *Y* only, and none of the two factors, respectively. The contributions of factor *X* and *Y* can be isolated as follows:

$$\boldsymbol{f}'_{\boldsymbol{X}} = \boldsymbol{f}_{\boldsymbol{X}} - \boldsymbol{f}_{\mathbf{0}}$$

$$\boldsymbol{f}'_{\boldsymbol{Y}} = \boldsymbol{f}_{\boldsymbol{Y}} - \boldsymbol{f}_{\mathbf{0}}$$

Note that term $\boldsymbol{f}'_{\boldsymbol{X}(\boldsymbol{Y})}$ represents the impacts of factor *X(Y)*, while $\boldsymbol{f}_{\mathbf{0}}$ is the term independent of factors *X* and *Y*.

The simulation including both factors *X* and *Y* is given by:

$$\boldsymbol{f}_{\boldsymbol{XY}} = \boldsymbol{f}_{\mathbf{0}} + \boldsymbol{f}'_{\boldsymbol{X}} + \boldsymbol{f}'_{\boldsymbol{Y}} + \boldsymbol{f}'_{\boldsymbol{XY}}$$

The mutual interaction between *X* and *Y* can be expressed as:

$$\boldsymbol{f}'_{\boldsymbol{XY}} = \boldsymbol{f}_{\boldsymbol{XY}} - \boldsymbol{f}_{\mathbf{0}} - \boldsymbol{f}'_{\boldsymbol{X}} - \boldsymbol{f}'_{\boldsymbol{Y}} = \boldsymbol{f}_{\boldsymbol{XY}} - (\boldsymbol{f}_{\boldsymbol{X}} - \boldsymbol{f}_{\mathbf{0}}) - (\boldsymbol{f}_{\boldsymbol{Y}} - \boldsymbol{f}_{\mathbf{0}}) - \boldsymbol{f}_{\mathbf{0}} = \boldsymbol{f}_{\boldsymbol{XY}} - \boldsymbol{f}_{\boldsymbol{X}} - \boldsymbol{f}_{\boldsymbol{Y}} + \boldsymbol{f}_{\mathbf{0}}$$

The above equation shows that the study needs four simulations, $\boldsymbol{f}_{\boldsymbol{XY}}, \boldsymbol{f}_{\boldsymbol{X}}, \boldsymbol{f}_{\boldsymbol{Y}}$ and $\boldsymbol{f}_{\mathbf{0}}$, to evaluate the contributions of two factors and their synergistic interactions.

SI-2.2 Statistical metrics for observation-model comparisons

In the present study, the mean bias (*MB*), root mean square error (*RMSE*) and the index of agreement (*IOA*) are used as indicators to evaluate the performance of WRF-CEHM model in simulation against measurements. *IOA* describes the relative difference between the model and observation, ranging from 0 to 1, with 1 indicating perfect agreement.

$$\boldsymbol{MB} = \frac{1}{N}\sum_{i=1}^{N}(\boldsymbol{P_i} - \boldsymbol{O_i})$$

$$\boldsymbol{RMSE} = \left[\frac{1}{N}\sum_{i=1}^{N}(\boldsymbol{P_i} - \boldsymbol{O_i})^2\right]^{\frac{1}{2}}$$

$$\boldsymbol{IOA} = 1 - \frac{\sum_{i=1}^{N}(\boldsymbol{P_i} - \boldsymbol{O_i})^2}{\sum_{i=1}^{N}(|\boldsymbol{P_i} - \overline{\boldsymbol{O}}| + |\boldsymbol{O_i} - \overline{\boldsymbol{O}}|)^2}$$

Where $\boldsymbol{P_i}$ and $\boldsymbol{O_i}$ are the predicted and observed pollutant concentrations, respectively. *N* is the total number of the predictions used for comparisons, and $\overline{\boldsymbol{P}}$ and $\overline{\boldsymbol{O}}$ represents the average of the prediction and observation, respectively.

Section SI-3 Synoptic patterns During the Study Episode

Figure S3 presents the mean geopotential heights with wind fields at 500 hPa from 23 to 28 May 2015. In May, the main part of the subtropical high at 500 hPa is located in the western Pacific, with its ridgeline moving around the south of China (Chang et al., 2000; Sui et al., 2007; Jiang et al., 2011). On 23 May 2015, a shallow trough was located between 120°E and 130°E, with the west-northwest wind prevailing over the NCP and its surroundings (Figure S3a). On 24 and 25 May 2015, the high-level trough intensified and moved to the east, the NCP was located behind the trough, and prevailing northwest winds dominate over the NCP (Figures S4b-c). From 26 to 28 May 2015, another weak trough was formed in the westerly wind zone and gradually intensified, moving from 120°E to 130°E. In general, during the study episode, the NCP and its surroundings were located behind the trough and northwest and west flows were prevailing across the region.

Figure S4 shows the variations of the daily mean sea level pressure and wind fields from 23 to 28 May 2015. During the study episode, eastern China was influenced by the high pressure whose center was located in the Yellow Sea, which was caused by the high-level trough. With the warm and humid flow induced by the Asian summer monsoon, rainstorms began to occur in the Pearl River Delta and Yangtze River Delta. The air quality in the NCP, NEC, and NWC was barely influenced by the precipitation during the episode. From 23 to 25 May 2015, when the NCP and its surroundings were located behind the high-level trough, most of the NCP and NWC regions were controlled by high pressures centering in the Yellow Sea. The high pressure system was conductive to the accumulation of air pollutants, increasing the O_3 and $PM_{2.5}$ levels in the NCP. Meanwhile, the low pressure system was stationed on the north of China. The Liaoning and Jilin provinces were located in the foreside of the low pressure system, and the prevailing southwest wind facilitated the transport of air pollutants from southwest to northeast. From 26 to 28 May, with the eastward movement of the high-level trough, the surface high pressure weather system began to be stagnant over eastern China, and most of the NCP regions were sandwiched between the high pressure located over the Yellow Sea and the deep low pressure lying in the north-south direction across Inner Mongolia and southern China. The resultant prevailing southeast and southwest winds were favorable for the air pollutants transport from the NCP to the NWC and NEC. In summary, under the effects of the low pressure in the continent and the high pressure over the Yellow Sea, the prevailing southeast or southwest winds over the NCP and its surroundings are expected to transport air pollutants from the NCP to the NEC and NWC.

Section SI-4 Evaluations of $PM_{2.5}$, O_3 and NO_2 Simulations in Northern China

The model generally reproduces the variations of $PM_{2.5}$, O_3 and NO_2 concentrations in Northern China, but the model biases still exist. To further evaluate the model performance, Table S1 shows the statistical comparisons of simulated and measured $PM_{2.5}$ concentrations of 13 provinces over NCP, NEC and NWC of China. Over the NCP, the model simulations in Hebei, Henan and Shandong are much better than the other provinces, with IOA_s of 0.87, 0.80 and 0.85, respectively. The obvious overestimations of $PM_{2.5}$ concentration occur in Beijing, Tianjin and Jiangsu, with *MB* of 10.3 μg m^{-3}, 10.7 μg m^{-3} and 10.4 μg m^{-3}, respectively. The model bias in Beijing is likely attributed to the trans-boundary transport (Wu et al., 2017). The overestimation in Tianjin and Jiangsu might be caused by the marine cloud and the convections, which can not be well resolved in the WRF-CHEM model simulations. The underestimation generally occurs in Anhui province, particular during the last three days, which is perhaps caused by uncertainties of the biomass burning emission. Over the NEC, the $PM_{2.5}$ concentrations in the four provinces are generally influenced by the trans-boundary transport from the NCP when southerly winds are prevailing. So the uncertainties of wind field simulations are one of the most important reasons for the model biases in modeling $PM_{2.5}$ concentrations in the NEC (Bei et al., 2010, 2016a, b). The model performs well in simulating the $PM_{2.5}$ concentration in Shanxi province in the NWC, with *IOA* and *MB* of 0.87 and -1.5 μg m^{-3}, respectively, but the overestimation occurs in Shaanxi province, with *IOA* and *MB* of 0.61 and 8.2 μg m^{-3}, possibly caused by the uncertainty of wind field simulations and the emission inventory.

Table S2 shows the statistical comparison of simulated and observed O_3 concentrations of 13 provinces in Northern China. The IOA_s of 7 provinces in the NCP are generally more than 0.90, except the Anhui Province, indicating the good model performance in the NCP, but the model is subject to underestimation, particular in Beijing which is influenced by the trans-boundary transport. The model simulation of O_3 concentrations in the NEC is not as good as that in the NCP, and the underestimation is considerable in Jilin, Liaoning and Inner Mongolia, which is plausibly caused by uncertainties of the trans-boundary transport of air pollutants from the NCP to NEC when the southerly wind is prevailing. The O_3 overestimation generally occurs in the NWC, with the *MB* of 7.5 μg m^{-3} and 11.8 μg m^{-3} in Shanxi and Shaanxi provinces, respectively. Table S3 provides the statistical comparison of simulated and observed NO_2 concentrations of 13 provinces in Northern China. The model simulations in Tianjin and Liaoning province are not very good in comparison with the other provinces, with the *IOA*s less than 0.50.

In general, the model can reasonably simulate the variation of air pollutants during the study episode, providing the basis to further investigate the effect of trans-boundary transport of the NCP emissions on the air quality in its surrounding provinces.

References

Bei, N., Lei, W., Zavala, M., and Molina, L. T.: Ozone predictabilities due to meteorological uncertainties in the Mexico City basin using ensemble forecasts, Atmospheric Chemistry and Physics, 10, 6295-6309, 10.5194/acp-10-6295-2010, 2010.

Bei, N. F., Li, G. H., Huang, R. J., Cao, J. J., Meng, N., Feng, T., Liu, S. X., Zhang, T., Zhang, Q., and Molina, L. T.: Typical synoptic situations and their impacts on the wintertime air pollution in the Guanzhong basin, China, Atmospheric Chemistry and Physics, 16, 7373-7387, 10.5194/acp-16-7373-2016, 2016a.

Bei, N. F., Xiao, B., Meng, N., and Feng, T.: Critical role of meteorological conditions in a persistent haze episode in the Guanzhong basin, China, Science of Total Environment, 550, 273-284, 10.1016/j.scitotenv.2015.12.159, 2016b.

Binkowski, F. S. and Roselle, S. J.: Models-3 Community Multiscale Air Quality (CMAQ) model aerosol component 1. Model description, J. Geophys. Res., 108(D6), 4183–18, doi:10.1029/2001JD001409, 2003.

Carnevale, C., Pisoni, E., and Volta, M.: A non-linear analysis to detect the origin of PM10 concentrations in Northern Italy, Science of Total Environment, 409, 182-191, 10.1016/j.scitotenv.2010.09.038, 2010.

Chang, C. P., Zhang, Y., and Li, T.: Interannual and Interdecadal Variations of the East Asian Summer Monsoon and Tropical Pacific SSTs. Part I: Roles of the Subtropical Ridge, Journal of Climate, 13, 4310-4325, 2000.

Chou, M. D., and Suarez, M. J.: A solar radiation parameterization for atmospheric studies, NASA TM-104606, Nasa Tech.memo, 15, 1999.

Chou, M. D., Suarez, M. J., Liang, X. Z., Yan, M. H., and Cote, C.: A Thermal Infrared Radiation Parameterization for Atmospheric Studies, Max J, 2001.

Gabusi, V., Pisoni, E., and Volta, M.: Factor separation in air quality simulations, Ecological Modelling, 218, 383-392, 10.1016/j.ecolmodel.2008.07.030, 2008.

Guenther, A., Karl, T., Harley, P., Wiedinmyer, C., Palmer, P. I., and Geron, C.: Estimates of global terrestrial isoprene emissions using MEGAN (Model of Emissions of Gases and Aerosols from Nature), Atmospheric Chemistry and Physics, 6, 3181-3210, 2006.

Hong, S.-Y., and Lim, J.-O. J.: The WRF Single-Moment 6-Class Microphysics Scheme (WSM6), Asia-Pacific Journal of Atmospheric Sciences, 42, 129-151, 2006.

Horowitz, L. W., Walters, S., Mauzerall, D. L., Emmons, L. K., Rasch, P. J., Granier, C., Tie, X. X., Lamarque, J. F., Schultz, M. G., Tyndall, G. S., Orlando, J. J., and Brasseur, G. P.: A global simulation of tropospheric ozone and related tracers: Description and evaluation of MOZART, version 2, Journal of Geophysical Research-Atmospheres, 108, 29, 10.1029/2002jd002853, 2003.

Jiang, X. W., Li, Y. Q., Yang, S., and Wu, R. G.: Interannual and interdecadal variations of the South Asian and western Pacific subtropical highs and their relationships with Asian-Pacific summer climate, Meteorology and Atmospheric Physics, 113, 171-180, 10.1007/s00703-011-0146-8, 2011.

Li, G. H., Zhang, R. Y., Fan, J. W., and Tie, X. X.: Impacts of black carbon aerosol on photolysis and ozone, Journal of Geophysical Research-Atmospheres, 110, 10, 10.1029/2005jd005898, 2005.

Li, G., Lei, W., Zavala, M., Volkamer, R., Dusanter, S., Stevens, P., and Molina, L. T.: Impacts of HONO sources on the photochemistry in Mexico City during the MCMA-2006/MILAGO Campaign, Atmospheric Chemistry and Physics, 10, 6551-6567, 10.5194/acp-10-6551-2010, 2010.

Li, G., Bei, N., Tie, X., and Molina, L. T.: Aerosol effects on the photochemistry in Mexico City during MCMA-2006/MILAGRO campaign, Atmospheric Chemistry and Physics, 11, 5169-5182, 10.5194/acp-11-5169-2011, 2011a.

Li, G., Zavala, M., Lei, W., Tsimpidi, A. P., Karydis, V. A., Pandis, S. N., agaratna, M. R., and Molina, L. T.: Simulations of organic aerosol concentrations in Mexico City using the WRF-CHEM model during the MCMA-2006/MILAGRO campaign, Atmospheric Chemistry and Physics, 11, 3789-3809, 10.5194/acp-11-3789-2011, 2011b.

Li, G. H., Bei, N. F., Zavala, M., and Molina, L. T.: Ozone formation along the California Mexican border region during Cal-Mex 2010 field campaign, Atmospheric Environment, 88, 370-389, 10.1016/j.atmosenv.2013.11.067, 2014a.

Nenes, A., Pandis, S. N., and Pilinis, C.: ISORROPIA: A new thermodynamic equilibrium model for multiphase multicomponent inorganic aerosols, Aquat. Geochem., 4, 123-152, 10.1023/a:1009604003981, 1998.

Stein, U., and Alpert, P.: Factor separation in numerical simulations, Journal of the Atmospheric Science, 50, 2107-2115, 10.1175/1520-0469(1993) 050<2107:fsins>2.0.co;2, 1993.

Sui, C. H., Chung, P. H., and Li, T.: Interannual and interdecadal variability of the summertime western North Pacific subtropical high, Geophysical Research Letters, 34, 6, 10.1029/2006gl029204, 2007.

Weinhold, B.: Ozone nation - EPA standard panned by the people, Environmental Health Perspectives, 116, A302-A305, 2008.

Wesely, M. L.: Parameterization of surface resistances to gaseous dry deposition in regional-scale numerical models, Atmospheric Environment, 23, 1293-1304, 10.1016/0004-6981(89)90153-4, 1989.

Wu, J., Li, G., Cao, J., Bei, N., Wang, Y., Feng, T., Huang, R., Liu, S., Zhang, Q., and Tie, X.: Contributions of trans-boundary transport to summertime air quality in Beijing, China, Atmospheric Chemistry and Physics, 17, 1-46, 2017.

Zhang, Q., Streets, D. G., Carmichael, G. R., He, K. B., Huo, H., Kannari, A., Klimont, Z., Park, I. S., Reddy, S., Fu, J. S., Chen, D., Duan, L., Lei, Y., Wang, L. T., and Yao, Z. L.: Asian emissions in 2006 for the NASA INTEX-B mission, Atmospheric Chemistry and Physics, 9, 5131-5153, 2009.

Table S1. Statistical comparison of simulated and measured $PM_{2.5}$ concentrations in the NCP, NEC and NWC.

Region	Province	*MB* (μg m^{-3})	*RMSE* (μg m^{-3})	*IOA*
NCP	Beijing	10.3	30.5	0.71
	Tianjin	10.7	33.3	0.52
	Hebei	7.5	14.4	0.87
	Shandong	-1.7	11.7	0.85
	Henan	2.3	21.5	0.80
	Jiangsu	10.4	18.9	0.44
	Anhui	-6.3	22.8	0.43
NEC	Liaoning	-1.5	12.6	0.67
	Jilin	-0.8	12.3	0.58
NWC	Shanxi	-1.5	14.8	0.87
	Shaanxi	8.2	14.6	0.61
NEC+NWC	Inner Mongolia	-11.5	15.4	0.60

Table S2. Statistical comparison of simulated and measured O_3 concentrations in the NCP, NEC and NWC.

Region	Province	*MB* (μg m^{-3})	*RMSE* (μg m^{-3})	*IOA*
NCP	Beijing	-18.6	46.0	0.90
	Tianjin	-13.6	33.3	0.90
	Hebei	-8.8	19.5	0.96
	Shandong	-14.4	22.5	0.94
	Henan	7.9	23.8	0.94
	Jiangsu	1.3	20.6	0.95
	Anhui	-6.3	22.8	0.84
NEC	Liaoning	-25.4	32.8	0.84
	Jilin	-23.2	34.8	0.83
NWC	Shanxi	7.5	21.3	0.94
	Shaanxi	11.8	23.3	0.89
NEC+NWC	Inner Mongolia	-13.7	19.3	0.92

Table S3. Statistical comparison of simulated and measured NO_2 concentrations in the NCP, NEC and NWC.

Region	Province	*MB* (μg m^{-3})	*RMSE* (μg m^{-3})	*IOA*
NCP	Beijing	5.0	17.7	0.66
	Tianjin	2.1	20.4	0.31
	Hebei	0.7	12.3	0.67
	Shandong	-0.5	12.3	0.71
	Henan	4.2	13.0	0.74
	Jiangsu	2.7	10.3	0.59
	Anhui	0.4	11.2	0.56
NEC	Liaoning	-0.8	12.7	0.45
	Jilin	3.3	12.2	0.68
NWC	Shanxi	1.7	11.5	0.79
	Shaanxi	4.7	11.1	0.75
NEC+NWC	Inner Mongolia	1.1	7.6	0.88

SI Figure Captions

Figure S1 Defined three sections in Northern China. 1) Northeast China (NEC): Heilongjiang, Jilin, Liaoning, and the east part of Inner Mongolia; 2) Northwest China (NWC): Shanxi, Shaanxi, and the west part of Inner Mongolia; 3) North China Plain (NCP): Beijing, Tianjin, Hebei, Shandong, Henan, and the north part of Jiangsu and Anhui.

Figure S2 Spatial distribution of anthropogenic emission rates of (a) NO_x, (b) VOC_s, (c) OC, and (d) SO_2 (10^6 g month^{-1}) in Mainland China.

Figure S3 Geopotential heights and wind vectors at 500 hPa from 23 to 28 May 2015.

Figure S4 The mean sea level pressure and wind vectors from 23 to 28 May 2015.

Figure S1 Defined three sections in Northern China. 1) Northeast China (NEC): Heilongjiang, Jilin, Liaoning, and the east part of Inner Mongolia; 2) Northwest China (NWC): Shanxi, Shaanxi, and the west part of Inner Mongolia; 3) North China Plain (NCP): Beijing, Tianjin, Hebei, Shandong, Henan, and the north part of Jiangsu and Anhui.

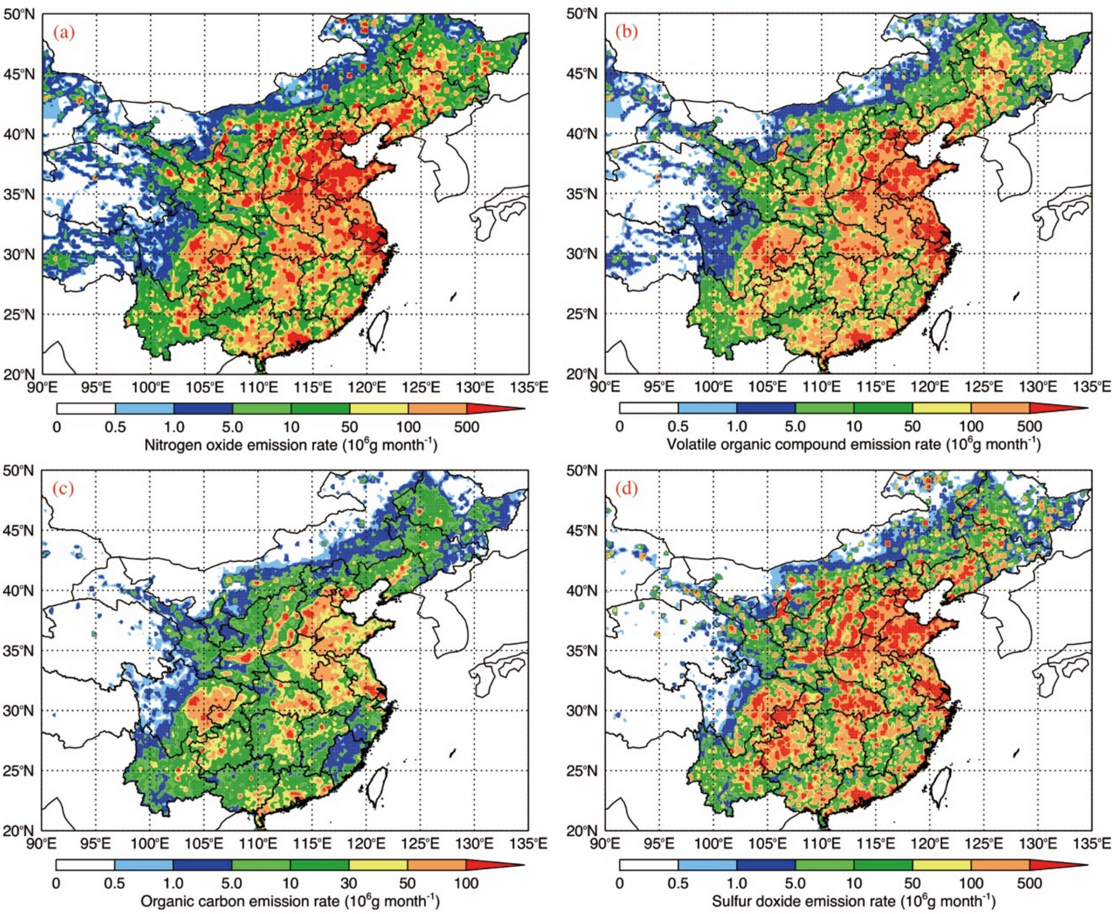

Figure S2 Spatial distribution of anthropogenic emission rates of (a) NO_x, (b) VOC_s, (c) OC, and (d) SO_2 (10^6 g $month^{-1}$) in Mainland China.

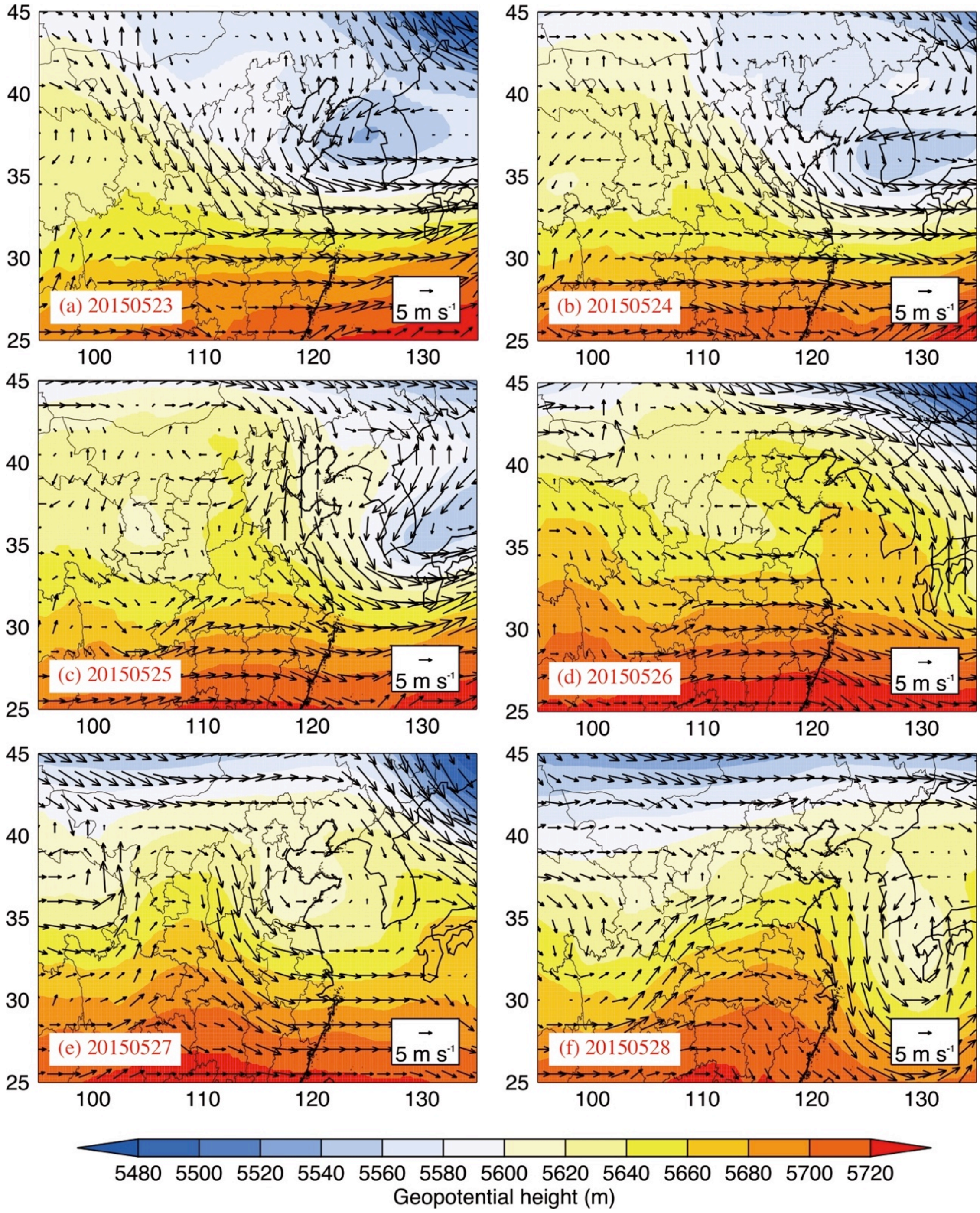

Figure S3 Geopotential heights and wind vectors at 500 hPa from 23 to 28 May 2015.

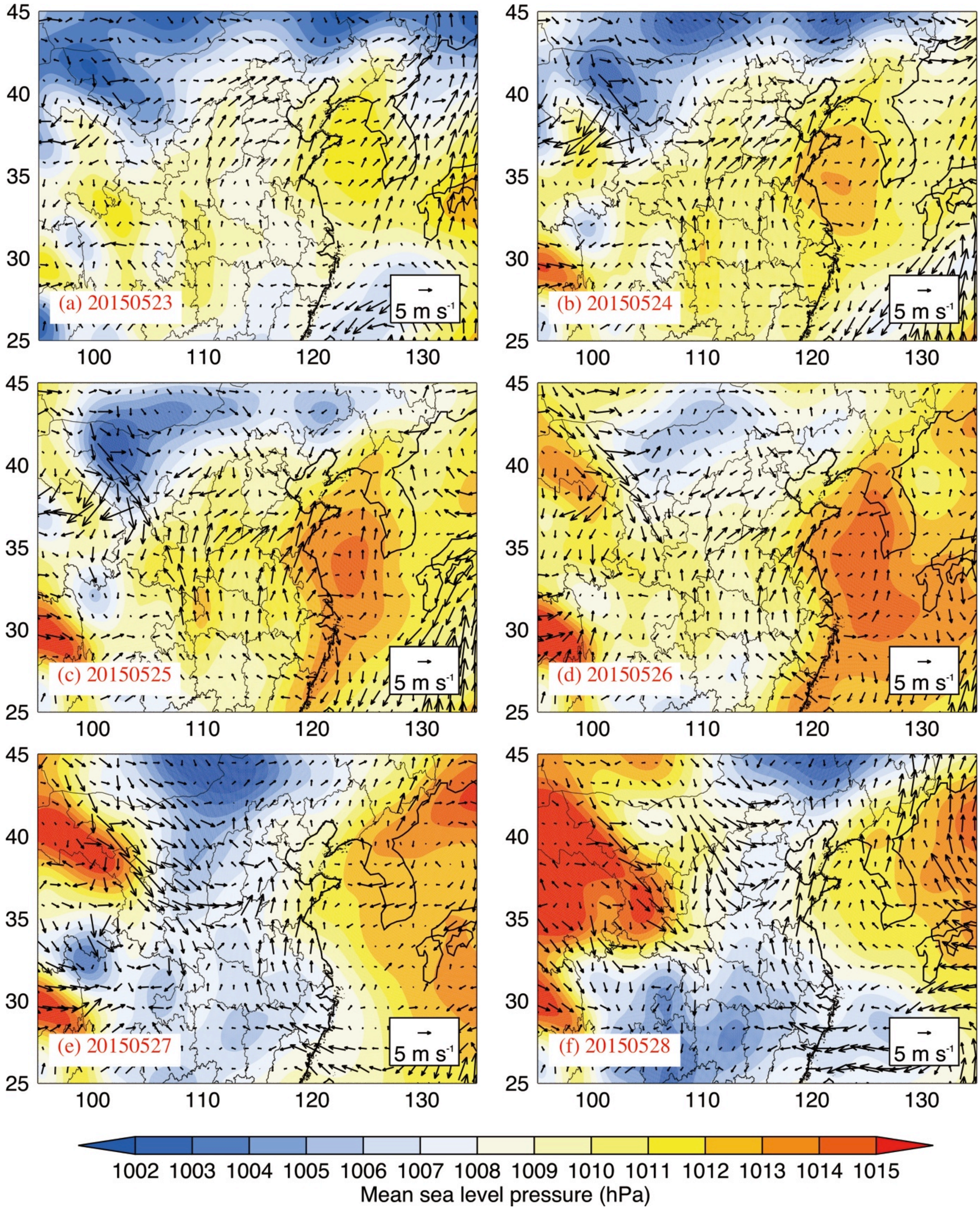

Figure S4 The mean sea level pressure and wind vectors from 23 to 28 May 2015.